

THE PLASTIC ZONE OF CLAY UNDER FOUNDATION LOAD: AN EXPERIMENTAL AND NUMERICAL ANALYSIS

Liu, X. H.; Jiang, S. Q.; Zeng, Y. Q.[#]; Hu, W. D.; Gong, Y. & Chen, J. L.

College of Civil Engineering and Architecture, Hunan Institute of Science and Technology,
414000, Yueyang, China

E-Mail: yqzeng@hnist.edu.cn ([#] Corresponding author)

Abstract

In order to study the generation and distribution of plastic zone of cohesive soil foundation with the change of foundation pressure and foundation width, particle image velocimetry testing technology and discrete element method are used to study the dynamic distribution characteristics of plastic zone of cohesive soil, foundation failure mode and corresponding foundation bearing capacity values. By using particle image velocimetry testing technology, the plastic zone of clay under different foundation load is obtained, in which the ultimate foundation bearing capacity can be taken as 120 kPa. The development law of foundation plastic zone simulated by UDEC is highly consistent with that of foundation plastic zone based on PIV test. Through the parameterized numerical simulation test of the foundation plastic zone, this paper discusses the variation law of foundation plastic zone with the changes in the foundation load and the width of foundation, which can be used to study the dynamic development process of plastic zone of the shallow foundation. The research has important guiding significance for evaluating the range of foundation plastic zone in foundation design.

(Received in December 2022, accepted in February 2023. This paper was with the authors 3 weeks for 2 revisions.)

Key Words: Plastic Zone, Foundation Bearing Capacity, Particle Image Velocimetry, Discrete Element Method

1. INTRODUCTION

As the foundation of architecture, the building foundation directly bears various loads from the superstructure; the quality of survey, design and construction on building foundation directly affects the normal use of architecture. In order to ensure the safety and good use of buildings [1-3], the following two technical conditions must be met at the same time in the foundation engineering design: (1) strength conditions: the building foundation is required to maintain stability without sliding failure, in which a certain foundation strength safety factor must be provided; (2) deformation condition: the foundation deformation of building shall not be greater than the allowable value specified in the normative standard. When the foundation meets strength and deformation conditions, the maximum foundation load that can be borne per unit area is called foundation bearing capacity [4-8]. Foundation bearing capacity is one of the classical theoretical problems of soil mechanics, which has a wide application background in construction, road and hydraulic engineering [9-12]. Experts and scholars pay more attention to the verification and development of traditional ultimate bearing capacity method, the traditional solutions mainly adopt limit equilibrium method and slip line method [13-15], which do not consider the stress-strain relationship of soil and take a specific slip surface shape as the premise, so it is difficult to get a reliable solution. The interaction between foundation and subgrade determines the settlement of structures and the foundation bearing capacity, which has been one of the main contents of soil mechanics and foundation engineering [16, 17]. Among the theoretical formulas for calculating the foundation bearing capacity, one is the formula for calculating the critical plastic load and critical load derived from the ultimate equilibrium condition of subgrade soil; the other is the formula for calculating the ultimate bearing capacity derived from the rigid plastic assumption of subgrade soil. In engineering practice, according to different requirements of buildings, the allowable bearing capacity of

foundation can be taken as the critical plastic load, critical load, or specific load divided by the ultimate bearing capacity formula with a certain safety factor [18, 19].

2. EXPERIMENTAL ANALYSIS ON PLASTIC ZONE OF CLAY

2.1 Foundation model box and vertical loading system

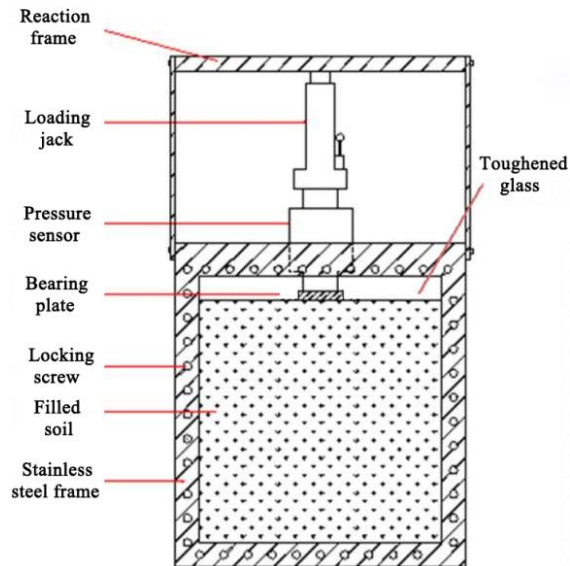


Figure 1: The schematic diagram of model box.

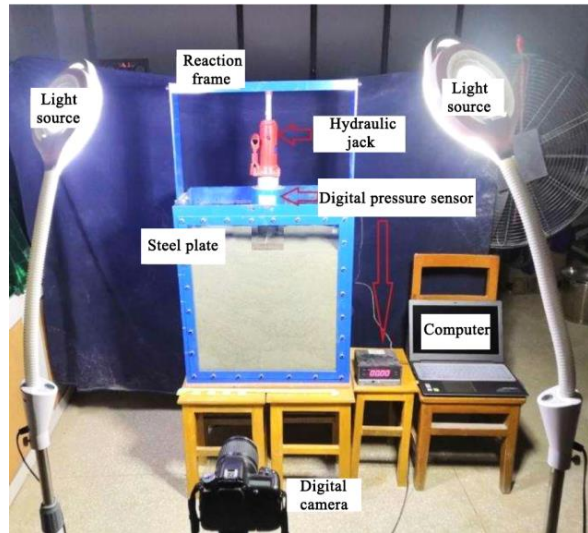


Figure 2: Test site of foundation plastic zone by PIV technique.

In model tests, the clay is taken as filling material, the schematic diagram of model box and test site of foundation plastic zone by PIV technique are shown in Figs. 1 and 2, respectively. The soil filled in the steel foundation model box is used to simulate the engineering subgrade. The steel structure model box is a cuboid, welded by steel plate and channel steel, in which the inner dimension of model box is 600 mm long, 335 mm wide and 1055 mm high. The front, back and top surfaces are open, and the left and right sides are 12 mm thick steel plates; where the top surface is open installed with an adjustable reaction frame, the front and back sides are 16 mm thick transparent tempered glass, which is convenient for directly viewing and taking photos of the load deformation process of foundation. The vertical loading system is composed of a reaction frame, hydraulic jack, pressure sensor, pressure-bearing steel plate, and dial indicator. The hydraulic jack is used to apply vertical pressure; a digital display pressure sensor with a maximum range of 500 kPa is placed axially between the hydraulic jack and the pressure-bearing steel plate, which can directly read the load of each level. The bearing steel plate placed on the filling soil surface with 300 mm long, 65 mm wide and 20 mm thick; it is assumed that the embedded depth of the foundation is zero.

2.2 Image acquisition and processing system

The image acquisition and processing system based on PIV technology is composed of LED shadowless light source, digital camera, computer and GOM Correlate image analysis software. The particle image velocimetry test system is shown in Fig. 2; the PIV test system can complete continuous photograph, image acquisition and image analysis. PIV technology takes a series of photos in real-time with a high-definition digital camera and uses GOM Correlate image analysis software to digitize all photos [20, 21]. The quantitative shear strain field and visual dynamic shear development process are obtained through continuous analysis of two consecutive digital images. During the plastic zone measurement, the PIV test system takes clay as the analysis object, the soil displacement is obtained by using a digital camera to take photos

automatically with a shooting interval of 1-2 seconds and is analysed by PIV analysis software. It should be known that the light source is placed on both sides of the test equipment to reduce mirror reflection.

2.3 Arrangement scheme for test

The main operation steps of foundation plastic zone test are as follows: (1) The clay with a certain ratio of width to height is filled in the foundation model box to simulate engineering subgrade. (2) A strip rigid bearing plate is placed on the surface of filled soil to simulate a rigid foundation, in which the width of rigid bearing plate is less than 1/3 of the width of filled soil to satisfy the condition of infinite soil mass. A hydraulic jack is vertically placed in the centre of the rigid bearing plate and the pressure sensor is placed between the hydraulic jack and the rigid bearing plate. (3) Turn off the indoor light and place one LED lamp on the left and right sides of transparent tempered glass surface to ensure that the surface has sufficient light. Place a high-definition camera in front, set the focal length, shooting frequency and take photos ahead of 5 s. (4) Vertical loading starts synchronously with high definition camera. In the process of gradually increasing the vertical load, the compressed and deformed soil in the box is photographed at a certain photographing frequency. The digital pressure sensor can accurately record the variation rules of the vertical load with time. (5) When the pressure sensor value drops sharply at a certain time point, it indicates that the stress state of soil has developed from the plastic deformation stage to the plastic flow stage, the experiment can be terminated. (6) Input the photos into the computer, process and analyse the whole process image of soil deformation by using GOM software, the soil displacement field in the box is obtained. According to the corresponding relationship between displacement and shear strain, convert the soil displacement field into shear strain field, the dynamic development process of plastic zone, the boundary line range and morphological characteristics of plastic zone can be observed visually. Finally, by analyse of the corresponding relationship between plastic zone and vertical load, the relationship between vertical load and displacement field, shear strain can be established.

2.4 Experimental results and analysis

The physical and mechanical indexes of clay are as follows: void ratio $e = 0.86$, natural moisture content $\omega = 27\%$, plastic limit moisture content $\omega_p = 22.5\%$, gravity $\gamma = 20 \text{ kN/m}^3$, internal friction angle $\varphi = 16$, cohesion $c = 25 \text{ kPa}$. In filling clay in the box, the clay is filled in layers with a thickness of 50 cm; the same standard is used for every layered compaction. The test starts after completing clay loading and standing for more than 24 hours.

After the loading and photographing of the foundation plastic zone, the continuous photos are analysed by GOM correlation image analysis software to obtain the corresponding shear strain nephogram when the foundation deformation reaches stability under different loads. As shown in Fig. 3, the measured distribution of the foundation plastic zone under different loads is obtained by using the pressure sensor and particle image velocimetry (PIV) testing technology.

From Fig. 3 a, it can be seen that the foundation soil first appears compression deformation under the action of a small external load of 20 kPa. The foundation soil is mainly compression deformation, the stress in the foundation is still in the elastic equilibrium stage, the shear stress at any point in the foundation is less than the shear strength, and there is no plastic zone in the foundation. In Figs. 3 b-d, it can be seen that with the increase of applied load from 20 kPa to 80 kPa, the foundation soil begins to appear local plastic zone at the bottom edges of both ends of the foundation. With the increase of load, the plastic zone deformation range of the soil under the foundation expands downward, and the lower parts of plastic zones on both sides gradually

close to the middle. Although plastic limit equilibrium occurs in some areas of the foundation soil, the plastic zone is not connected; the foundation still has a certain stability, but the foundation's safety decreases with the plastic zone's expansion. According to Figs. 4 e-h, it can be seen that with the increase of applied load from 90 kPa to 120 kPa, the plastic zone of the foundation on both sides below the foundation penetrates to form a continuous failure surface, the intersection range of the plastic zone on both sides increases, at the same time, the soil on both sides of foundation heaves upper; Fig. 4 i indicate that a small load increment will cause large deformation of the foundation. This deformation is not caused by soil compression, but due to the plastic flow of the foundation soil. It is an unstable deformation with time. As a result, the foundation collapses to the weaker side, and the whole foundation loses stability; the foundation is subject to settlement failure to the left, in which the ultimate bearing capacity of the foundation can be taken as 120 kPa.

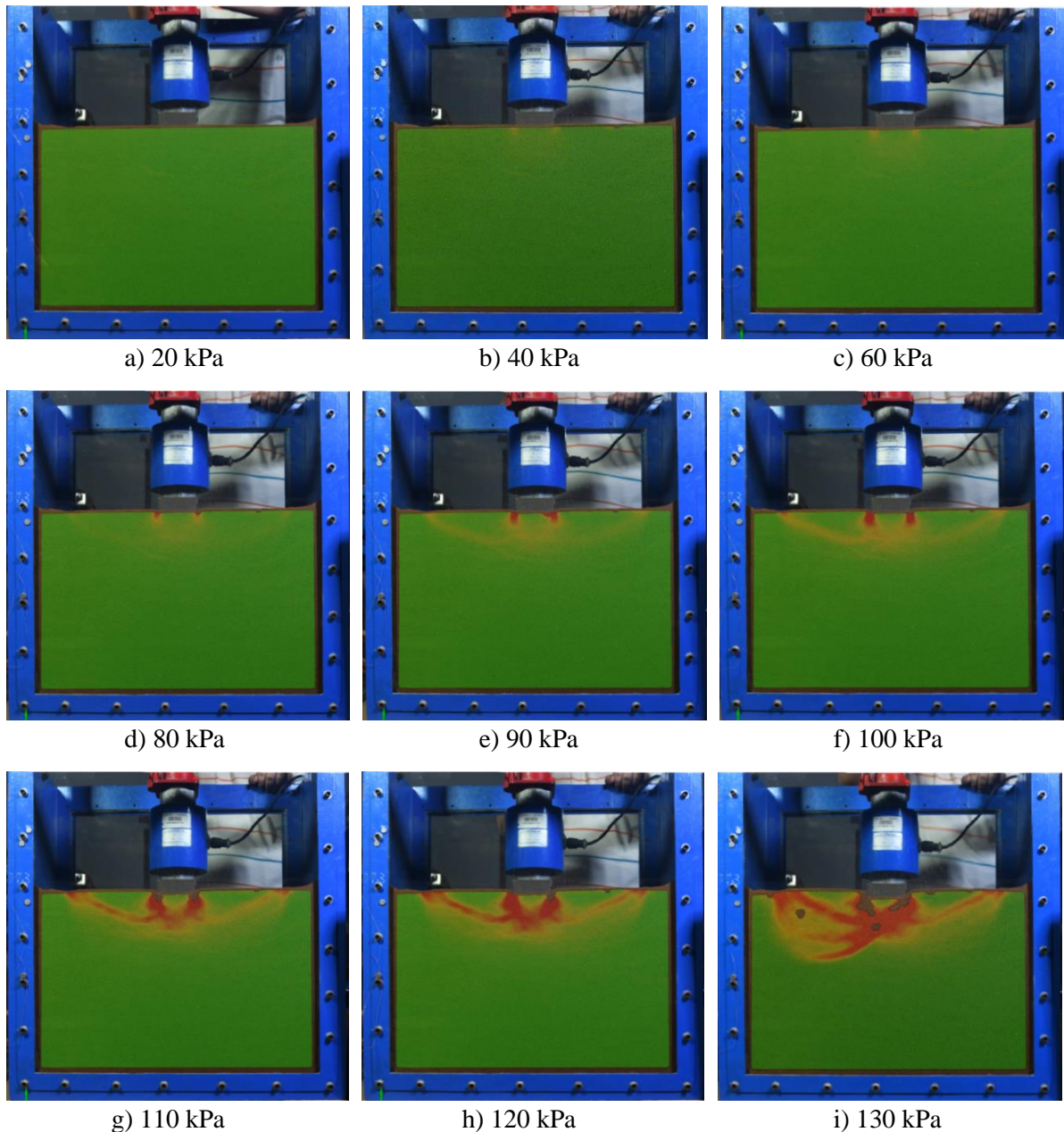


Figure 3: The measured distribution of foundation plastic zone under different loads.

3. NUMERICAL ANALYSIS ON PLASTIC ZONE OF CLAY

3.1 Model building of numerical simulation

Based on the above PIV test in the plastic zone of foundation, a numerical calculation model is established through UDEC 6.0. The geometric model dimensions of soil studied by UDEC are shown in Fig. 4; the horizontal width and vertical height of soil are set as 0.78 m and 0.36 m, respectively; the width and thickness of bearing steel plate are 0.065 m and 0.02 m, respectively. Therefore, the soil width ratio to the bearing steel plate is 12, and the ratio of the soil height to the width of the bearing steel plate is 5.5, which can better eliminate the influence of soil boundary constraint state on the plastic zone of foundation. The boundary conditions on both sides and bottom of the numerical model are fixed by displacement; the boundary condition of the model is that the bottom boundary has no horizontal and vertical displacement, and the left and right boundaries have no horizontal displacement; in addition, the upper boundary of the model is a free boundary, which can be loaded through bearing steel plate to simulate the load of the building. Due to the uniform soil is used in the study area, the internal structure of soil is relatively simple, so only the gravity stress of soil is considered and the effect of tectonic stress is not considered.

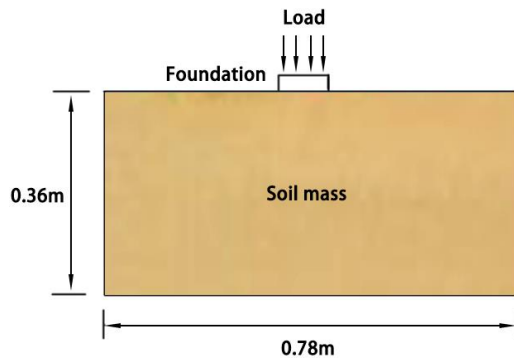


Figure 4: Schematic diagram of numerical calculation model for foundation plastic zone.

The physical and mechanical indexes of clay are shown in Table I. The joint model parameters generated and assigned by UDEC-Voronoi are shown in Table II.

Table I: The physical and mechanical indexes of clay.

Density (kg/m ³)	Elastic modulus (MPa)	Poisson ratio	Cohesion (kPa)	Internal friction angle (°)	Tensile strength (kPa)
2000	30	0.23	25	16	15.1

Table II: Voronoi randomly distributed joint characteristic parameters.

Normal stiffness (Pa/m)	Tangential stiffness (Pa/m)	Cohesion (kPa)	Internal friction angle (°)	Tensile strength (kPa)
9 e11	9 e11	0	15	0

The foundation vertical displacement curve under different loads is shown in Fig. 5. It can be seen from Fig. 5 that the foundation moves downward with the increase of load, the soil mass at the bottom and both sides of the foundation also move downward. It can be seen that the maximum displacement of soil mass is found at the bottom of foundation. When the load is 20 kPa, 50 kPa, 80 kPa, 100 kPa, 120 kPa, 130 kPa, 140 kPa, 150 kPa, 160 kPa and 170 kPa, the maximum displacement values are 0.0752 mm, 0.1449 mm, 0.1923 mm, 0.2017 mm, 0.2584

mm, 0.3763 mm, 0.4319 mm, 0.6342 mm, 0.7717 mm and 0.9820 mm; when the foundation load is 20~120 kPa, the vertical displacement slowly increases with the increase of load. When the load exceeds 120 kPa, the foundation vertical displacement increases significantly. Therefore, the ultimate load of foundation bearing capacity can be taken as 120 kPa, which is consistent with the ultimate bearing capacity of the foundation in the plastic zone test in Fig. 3.

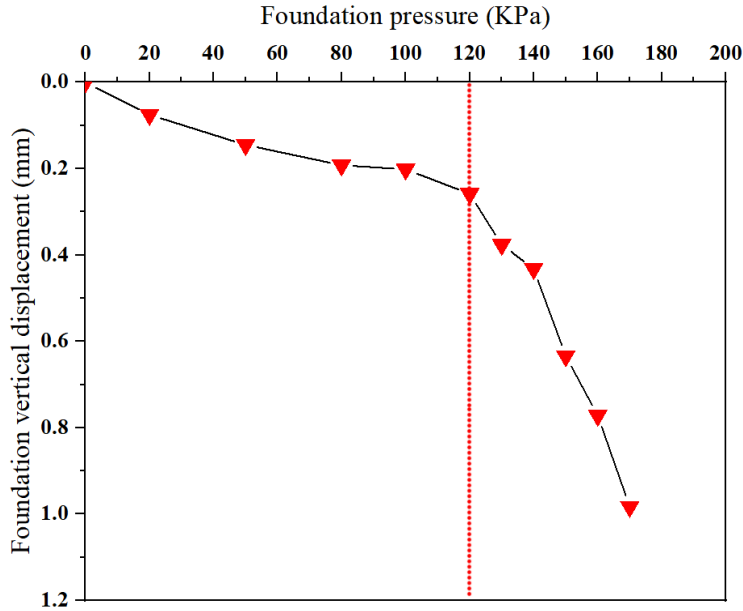


Figure 5: Foundation vertical displacement curve under different loads.

The distribution range and location of the plastic zone is an important index to measure the stability of soil mass. Fig. 6 shows the soil mass's plastic zone distribution under different loads. It can be seen from Fig. 6 a that when the foundation load is 20 kPa, the plastic zone of the foundation is tiny, and the foundation has only slight plastic deformation. As can be seen from Fig. 6 b-d that when the foundation load is 50 kPa, 80 kPa and 100 kPa, respectively, the plastic zone of foundation gradually appears on both sides of the foundation, but no connecting area is formed. In Fig. 6 e, it can be seen that when the foundation load is 120 kPa, a large number of foundation plastic zones are formed below the foundation, and a connected foundation plastic zone is formed; in addition, it can be seen from Fig. 6 f-j that when the load is increased from 130 kPa to 170 kPa, the plastic zone of the foundation is further expanded and extends around. The development law of the foundation plastic zone simulated by UDEC is highly consistent with that of the foundation plastic zone based on the PIV test shown in Fig. 3, which indicates that UDEC can better simulate the development law of foundation plastic zone.

3.2 Parametric study on plastic zone of clay

According to the above analysis results, the size and distribution range of the foundation plastic zone is affected by the width of foundation and the size of foundation load. In order to study the variation law of the foundation plastic zone with the width of the foundation and the size of foundation load, a parametric analysis is conducted. The foundation width is 0.5 m, 0.75 m, 1 m, 1.25 m and 1.5 m, respectively; the foundation load is 25 kPa, 75 kPa, 125 kPa, 175 kPa and 225 kPa, respectively. Through parametric study, the quantitative relationship of the influence of the width of foundation and the size of foundation load on the depth of plastic zone on foundation bottom, the width of plastic zone on both sides of foundation, the ratio for the depth of plastic zone to the width of foundation, the ratio for the width of plastic zone to the width of foundation, and the ratio for the width of plastic zone to the depth of plastic zone are obtained.



Figure 6: The distribution of the plastic zone of soil mass under different load.

3.3 Numerical simulation results and discussion

The variation of plastic zone depth and plastic zone width under different foundation loads is shown in Fig. 7. It can be seen from Fig. 7 that for the foundation width of 0.5 m, 0.75 m, 1.0 m, 1.25 m, 1.5 m, the plastic zone depth and width show the same rule with the change of foundation load, that is, when the load is 25 kPa, the plastic zone depth and width are both at small values in the range of 0.05~0.16 m and 0.11~0.33 m, respectively. When the foundation load increases from 25 kPa to 75 kPa, the depth and width of plastic zone increase significantly;

subsequently, as the foundation load gradually increases from 75 kPa to 225 kPa, the plastic zone depth and width show a similar linear increase trend; as a result, the plastic zone depth range increases from 0.53~1.54 m to 1.16~3.13 m, and the plastic zone width range increases from 0.98~3.04 m to 2.12~6.27 m.

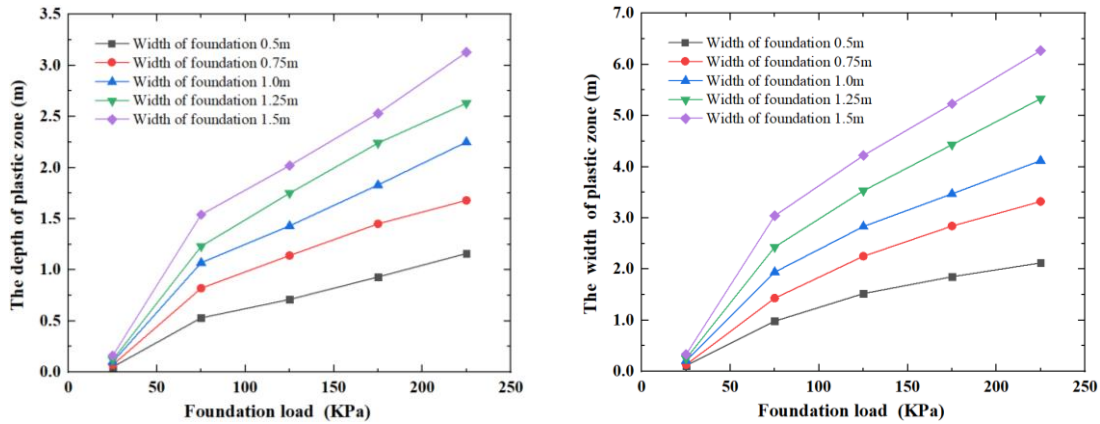


Figure 7: The variation of plastic zone depth and plastic zone width under different foundation load.

The variation of plastic zone depth and plastic zone width under different foundation widths is shown in Fig. 8. It can be seen from Fig. 8 that when the base pressure is 25 kPa, 75 kPa, 125 kPa, 175 kPa and 225 kPa, the variation of the plastic zone depth and plastic zone width with the foundation width shows the same rule; that is, when the foundation width increases from 0.5 m to 1.5 m, the plastic zone depth and plastic zone width show a similar linear increase trend, the plastic zone depth range increases from 0.05~1.16 m to 0.16~3.13 m, and the plastic zone width range increases from 0.11~2.12 m to 0.33~6.27 m.

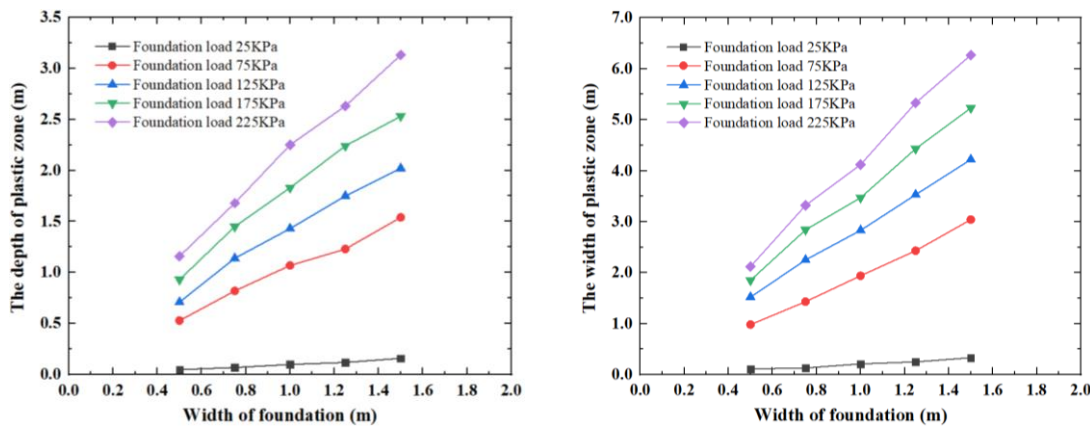


Figure 8: The variation of plastic zone depth and plastic zone width under different foundation width.

The variation of the ratio for depth of plastic zone to width of foundation and the ratio for width of plastic zone to width of foundation under different foundation loads is shown in Fig. 9. It can be seen from Fig. 9 that when the foundation width is 0.5 m, 0.75 m, 1.0 m, 1.25 m and 1.5 m, the ratio for depth of plastic zone to width of foundation and the ratio for width of plastic zone to width of foundation have the same rule, that is, when the load is 25 kPa, the ratio for depth of plastic zone to width of foundation and the ratio for width of plastic zone to width of foundation are both small in the range of 0.09~0.11 and 0.17~0.22, respectively. When the base load increases from 25 kPa to 75 kPa, the ratio for depth of plastic zone to width of foundation and the ratio for width of plastic zone to width of foundation has a significant increase. Thereafter, as the base load gradually increases from 75 kPa to 225 kPa, the ratio for depth of plastic zone to width of foundation and the ratio for width of plastic zone to width of foundation

show a similar linear increase trend, the ratio for depth of plastic zone to width of foundation increases from 0.98~1.09 to 2.09~2.32, the ratio for width of plastic zone to width of foundation increases from 1.91~2.03 to 4.12~4.43.

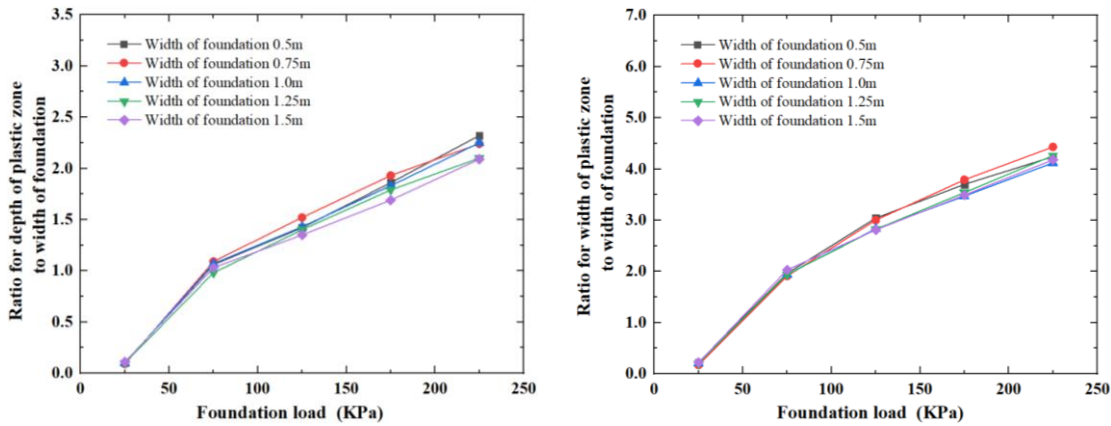


Figure 9: The variation of the ratio for depth of plastic zone to width of foundation and the ratio for width of plastic zone to width of foundation under different foundation load.

The variation of the ratio for depth of plastic zone to width of foundation and the ratio for width of plastic zone to width of foundation under different foundation widths is shown in Fig. 10. It can be seen in Fig. 10 that for the base pressure is 25 kPa, 75 kPa, 125 kPa, 175 kPa and 225 kPa, the value of the ratio for depth of plastic zone to width of foundation and the ratio for width of plastic zone to width of foundation approximately keeps stable with the increase of foundation width. When the foundation width increases from 0.5 m to 1.5 m, the ratio for depth of plastic zone to width of foundation ranges from 0.10~2.32 to 0.11~2.09, the ratio for width of plastic zone to width of foundation ranges from 0.22~4.24 to 0.22~4.18.

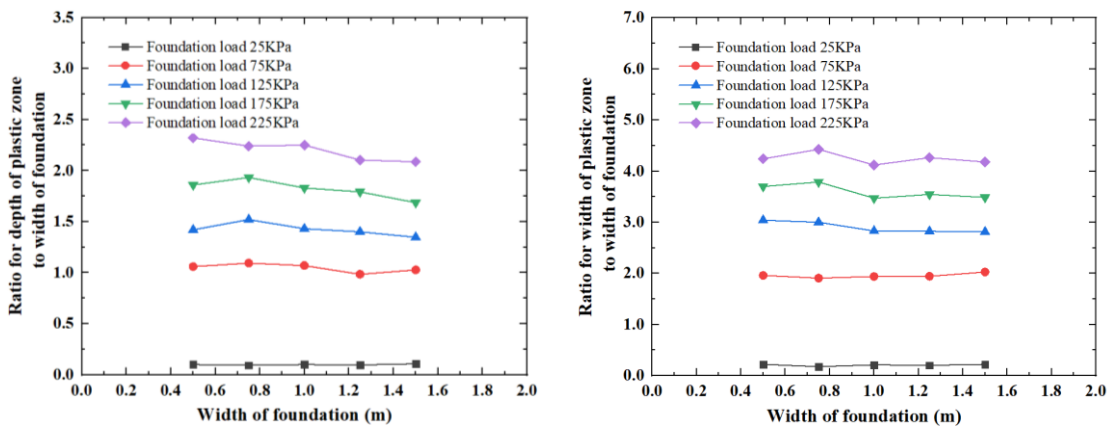


Figure 10: The variation of the ratio for depth of plastic zone to width of foundation and the ratio for width of plastic zone to width of foundation under different foundation width.

The variation of the ratio for width of plastic zone to depth of plastic zone with different foundation loads and different foundation widths is shown in Figs. 11 and 12, respectively. It can be seen from Figs. 11 and 12 that the variation curves about the ratio for the width of plastic zone to the depth of plastic zone with different foundation load and different foundation width both show an approximately horizontal state; that is, as the foundation load increases from 25 kPa to 225 kPa, the foundation width increases from 0.5 m to 1.5 m, the ratio for the width of plastic zone to the depth of plastic zone changes slightly. Fig. 11 shows that for foundation widths of 0.5 m, 0.75 m, 1.0 m, 1.25 m and 1.5 m, as the foundation load increases from 25 kPa to 225 kPa, the ratio for the width of plastic zone to the depth of plastic zone changes from

1.86~2.20 to 1.83~2.00. Fig. 12 shows that for the foundation load pressure of 25 kPa, 75 kPa, 125 kPa, 175 kPa and 225 kPa, as the foundation width increases from 0.5 m to 1.5 m, the ratio for the width of plastic zone to the depth of plastic zone varies from 1.83~2.20 to 2.00~2.06.

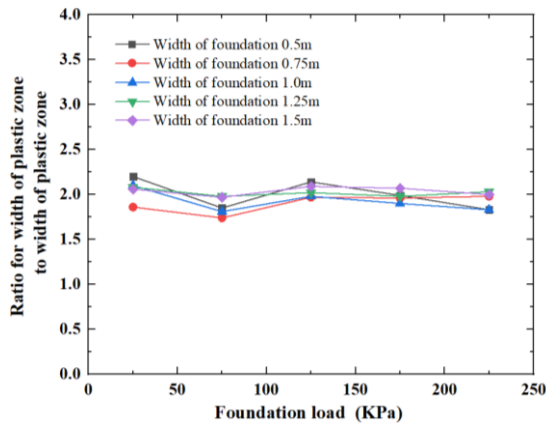


Figure 11: The variation of the ratio for width of plastic zone to depth of plastic zone under different foundation load.

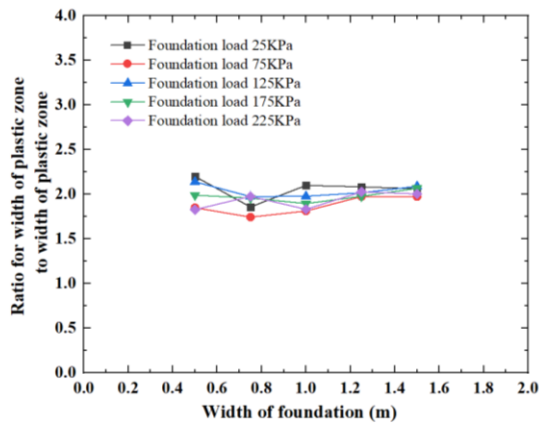


Figure 12: The variation of the ratio for width of plastic zone to depth of plastic zone under different foundation width.

4. CONCLUSION

Aiming at the shallow foundation, the particle image velocimetry (PIV) technique and discrete element method are used to study the dynamic quantitative characteristics of the plastic zone, foundation failure mode and corresponding foundation bearing capacity values. Based on the PIV test in the plastic zone of foundation, a numerical calculation model is established through UDEC 6.0. The main conclusions are drawn as follows:

- 1) This paper introduces in detail the test device and the test procedure of foundation plastic zone, including the foundation model box and vertical loading system, image acquisition and processing system, and arrangement scheme for the test, which can excellently meet the test requirements.
- 2) For analysing the plastic zone with the particle image velocimetry technique, the foundation soil first appears compression deformation under the action of a small external load of 20 kPa. With the increase of applied load from 20 kPa to 80 kPa, the foundation soil begins to appear local plastic zone at the bottom edges of both ends of the foundation. With the increase of load, the plastic zone deformation range of the soil under the foundation expands downward, and the lower parts of plastic zones on both sides gradually close to the middle. With the increase of applied load from 90 kPa to 120 kPa, the plastic zone of the foundation on both

sides below the foundation penetrates to form a continuous failure surface; finally, a small load increment will cause large deformation of the foundation. This deformation is not caused by soil compression, but due to the plastic flow of the foundation soil. As a result, the foundation collapses to the weaker side and the whole foundation loses stability; the foundation is subject to settlement failure to the left, in which the ultimate bearing capacity of the foundation can be taken as 120 kPa.

3) For analysing the plastic zone with the discrete element method, the development law of foundation plastic zone simulated by UDEC is highly consistent with that of the foundation plastic zone based on the PIV test, which shows that UDEC can better simulate the development law of foundation plastic zone. By conducting parameterized numerical simulation test for the plastic zone of foundation and analysing the results, with the changes in the foundation load and the width of foundation, the variation law of (1) the depth of plastic zone on foundation bottom, (2) the width of plastic zone on both sides of foundation, (3) the ratio for the depth of plastic zone to the width of foundation, (4) the ratio for the width of plastic zone to the width of foundation and (5) the ratio for the width of plastic zone to the depth of plastic zone is obtained.

In this study, the evolution mode of mechanical mechanism in the development process of the foundation plastic zone is discussed. Through the parameterized numerical simulation test of the foundation plastic zone, this paper discusses the variation law of the foundation plastic zone with the changes of the foundation load and the width of foundation, which can be used to study the dynamic development process of the plastic zone of the shallow foundation. The proposed method can provide theoretical and data support for determining the ultimate bearing capacity of the foundation.

ACKNOWLEDGEMENT

The study was supported by the Natural Science Foundation of Hunan Province of China (Grants 2017JJ2110 and 2022JJ40160), the Key Scientific Program of Hunan Education Department, China (Grant No. 20A228 and Grant No. 22A0472), the Postgraduate Scientific Research Innovation Project of Hunan Institute of Science and Technology (Grant No. 2022-080 and Grant No. 2022-081), the Teaching Reform Research Project of Hunan Institute of Science and Technology (Grant No. 2022A34), the Teaching Reform Research Project of Hunan Province Education Department, China (Grant No. HNJG-2022-0904), the Innovation Project of Hunan Undergraduate Students (Grant No. S202210543054 and Grant No. S202210543057) and the National Innovation and Entrepreneurship Training Program for Undergraduate Students (Grant No. 202210543054).

REFERENCES

- [1] Chen, H. H.; Zhu, H. H.; Zhang, L. Y. (2022). An analytical approach to the ultimate bearing capacity of smooth and rough strip foundations on rock mass considering three-dimensional (3D) strength, *Computers and Geotechnics*, Vol. 149, Paper 104865, 11 pages, doi:[10.1016/j.compgeo.2022.104865](https://doi.org/10.1016/j.compgeo.2022.104865)
- [2] Kumar, J.; Chakraborty, M. (2015). Bearing capacity of a circular foundation on layered sand-clay media, *Soils and Foundations*, Vol. 55, No. 5, 1058-1068, doi:[10.1016/j.sandf.2015.09.008](https://doi.org/10.1016/j.sandf.2015.09.008)
- [3] Shaunik, D.; Singh, M. (2020). Bearing capacity of foundations on rock slopes intersected by non-persistent discontinuity, *International Journal of Mining Science and Technology*, Vol. 30, No. 5, 669-674, doi:[10.1016/j.ijmst.2020.03.018](https://doi.org/10.1016/j.ijmst.2020.03.018)
- [4] Gao, J. L.; Liu, L.; Zhang, Y. P.; Xie, X. L. (2022). Deformation mechanism and soil evolution analysis based on different types geogrid reinforced foundation, *Construction and Building Materials*, Vol. 331, Paper 127322, 14 pages, doi:[10.1016/j.conbuildmat.2022.127322](https://doi.org/10.1016/j.conbuildmat.2022.127322)
- [5] Benmebarek, S.; Saifi, I.; Benmebarek, N. (2017). Depth factors for undrained bearing capacity of circular footing by numerical approach, *Journal of Rock Mechanics and Geotechnical Engineering*, Vol. 9, No. 4, 761-766, doi:[10.1016/j.jrmge.2017.01.003](https://doi.org/10.1016/j.jrmge.2017.01.003)

- [6] Peng, M.-X.; Peng, H.-X. (2019). The ultimate bearing capacity of shallow strip footings using slip-line method, *Soils and Foundations*, Vol. 59, No. 3, 601-616, doi:[10.1016/j.sandf.2019.01.008](https://doi.org/10.1016/j.sandf.2019.01.008)
- [7] Tan, M. X.; Vanapalli, S. K. (2022). Foundation bearing capacity estimation on unsaturated soil slope under transient flow condition using slip line method, *Computers and Geotechnics*, Vol. 148, Paper 104804, 16 pages, doi:[10.1016/j.compgeo.2022.104804](https://doi.org/10.1016/j.compgeo.2022.104804)
- [8] Santhoshkumar, G.; Ghosh, P. (2020). Ultimate bearing capacity of skirted foundation on cohesionless soil using slip line theory, *Computers and Geotechnics*, Vol. 123, Paper 103573, 9 pages, doi:[10.1016/j.compgeo.2020.103573](https://doi.org/10.1016/j.compgeo.2020.103573)
- [9] Kasama, K.; Whittle, A. J.; Kitazume, M. (2019). Effect of spatial variability of block-type cement-treated ground on the bearing capacity of foundation under inclined load, *Soils and Foundations*, Vol. 59, No. 6, 2125-2143, doi:[10.1016/j.sandf.2019.11.007](https://doi.org/10.1016/j.sandf.2019.11.007)
- [10] Rizvi, S. M. F.; Wang, K. H.; Jalal, F. E.; Wu, J. T.; Dong, M.; Tu, Y.; Zhao, S. (2022). Evaluation of capacity of power hammer machine foundation from high strain dynamic load test: field test and axisymmetric numerical modeling, *Transportation Geotechnics*, Vol. 36, Paper 100826, 19 pages, doi:[10.1016/j.trgeo.2022.100826](https://doi.org/10.1016/j.trgeo.2022.100826)
- [11] Chwała, M.; Kawa, M. (2021). Random failure mechanism method for assessment of working platform bearing capacity with a linear trend in undrained shear strength, *Journal of Rock Mechanics and Geotechnical Engineering*, Vol. 13, No. 6, 1513-1530, doi:[10.1016/j.jrmge.2021.06.004](https://doi.org/10.1016/j.jrmge.2021.06.004)
- [12] Pieczyńska-Kozłowska, J.; Vessia, G. (2022). Spatially variable soils affecting geotechnical strip foundation design, *Journal of Rock Mechanics and Geotechnical Engineering*, Vol. 14, No. 3, 886-895, doi:[10.1016/j.jrmge.2021.10.010](https://doi.org/10.1016/j.jrmge.2021.10.010)
- [13] Rahaman, O.; Kumar, J. (2022). Seismic bearing capacity of a strip footing on rock media, *Journal of Rock Mechanics and Geotechnical Engineering*, Vol. 14, No. 2, 560-575, doi:[10.1016/j.jrmge.2021.08.017](https://doi.org/10.1016/j.jrmge.2021.08.017)
- [14] Nguyen, H. C.; Vo-Minh, T. (2022). The use of the node-based smoothed finite element method to estimate static and seismic bearing capacities of shallow strip footings, *Journal of Rock Mechanics and Geotechnical Engineering*, Vol. 14, No. 1, 180-196, doi:[10.1016/j.jrmge.2021.11.005](https://doi.org/10.1016/j.jrmge.2021.11.005)
- [15] Wang, L. Z.; Shu, H. (2010). Application of Hill's stability condition to bearing capacity computation of foundation with finite element method, *Proceedings of the 11th National Conference on Rock Mechanics and Engineering*, 540-549
- [16] Liu, L. L.; Huang, M. S. (2010). Bearing capacity behaviours and failure modes of foundation under highway subgrade, *Chinese Journal of Underground Space and Engineering*, Vol. 6, No. 1, 84-89
- [17] Jiang, A. N.; Tang, C. A. (2010). Limit analysis and bearing capacity safety research for foundation with under soft layer using numerical experiment, *Rock and Soil Mechanics*, Vol. 31, No. 3, 956-960
- [18] Wang, D. Y.; Chen, X.; Yu, Y. Z.; Lu, Y. N. (2019). Ultimate bearing capacity analysis of shallow strip footing based on second-order cone programming optimized incremental loading finite element method, *Rock and Soil Mechanics*, Vol. 40, No. 12, 4890-4896
- [19] Liu, Y.; Fan, W. G.; Zhang, X. L.; Wu, Z. W.; Wu, C. X. (2022). Static contact modelling and analysis for rail grinding with abrasive belt, *International Journal of Simulation Modelling*, Vol. 21, No. 3, 513-524, doi:[10.2507/IJSIMM21-3-CO13](https://doi.org/10.2507/IJSIMM21-3-CO13)
- [20] Hu, W. D.; Zhu, Z. X.; Zeng, Y. Q.; Liu, X. H.; Peng, C. C. (2022). Active earth pressure against flexible retaining wall for finite soils under the drum deformation mode, *Scientific Reports*, Vol. 12, Paper 497, 25 pages, doi:[10.1038/s41598-021-04411-4](https://doi.org/10.1038/s41598-021-04411-4)
- [21] Zhu, X. N.; Zeng, Y. Q.; Hu, W. D.; Liu, X. H.; Zhou, X. Y. (2021). Experimental study on passive earth pressure against flexible retaining wall with drum deformation, *Engineering Letters*, Vol. 29, No. 2, 339-350